Research in Astronomy and Astrophysics, 24:115001 (10pp), 2024 November https://doi.org/10.1088/1674-4527/ad7fb6

Single-pulse Emissions of PSRs J1611–0114 and J1617+1123

Shifang Liu[1,2], Zhigang Wen[2,3,4], Shuangqiang Wang[2,3], Feifei Kou[2,4], Wenming Yan[2,3,4], Jianping Yuan[1,2,3], Qingdong Wu[2,3], De Zhao[1,2], Chenchen Miao[5], Na Wang[1,2,3], Menyao Xue[5], Di Li[5,6], Pei Wang[5], Shengnan Sun[2], Weiwei Zhu[5], and Juntao Bai[2,3]
[1] School of Physics and Technology, Xinjiang University, Urumqi 830046, China; yuanjp@xao.ac.cn
[2] Xinjiang Astronomical Observatory, Chinese Academy of Sciences, Urumqi 830046, China
[3] University of Chinese Academy of Sciences, Beijing 100049, China
[4] Xinjiang Key Laboratory of Radio Astrophysics, Urumqi 830046, China
[5] National Astronomical Observatories, Chinese Academy of Sciences, Beijing 100101, China
[6] Department of Astronomy, Tsinghua University, Beijing 100084, China
Received 2024 April 24; revised 2024 August 31; accepted 2024 September 23; published 2024 October 17

Abstract

In this paper, the emissions from two pulsars, PSRs J1611−0114 and J1617+1123, were investigated using the Five-hundred-meter Aperture Spherical radio Telescope operating at a central frequency of 1250 MHz. The average pulse profile of PSR J1611−0114 shows two components, the first of which is relatively weak in intensity. The two-dimensional pulse stack exhibits an obvious nulling phenomenon, with an estimated nulling fraction of $40.1\% \pm 5.4\%$. The durations of the nulls and bursts are consistent with power-law distributions, and no periodic nulling phenomenon is found. The results from PSR J1617+1123 demonstrate that the average pulse profile is composed of four components. The peak intensity of the fourth component varies significantly, causing an unstable integrated profile. In addition, the modulation characteristics of J1611−0114 and J1617+1123 were studied by analyzing the modulation index, longitude resolved fluctuation spectrum and two-dimensional fluctuation spectrum using the software PSRSALSA. It was found that the two pulsars exhibit intensity modulation. In particular, J1611−0114 displays even–odd modulation, with the modulation period of approximately two pulses. The modulation period of J1617+1123 is relatively broad. There is an obvious subpulse drift phenomenon, and the value of P_2 is $\sim 0.125c/P_0$, corresponding to 12 pulse longitude bins, and the drift rate (P_2/P_3) is about 0.29.

Key words: stars: neutron – (stars:) pulsars: general – (stars:) pulsars: individual (PSRs J1611−0114 and J1617+1123)

1. Introduction

Pulsars are rapidly rotating neutron stars with a strong magnetic field. They can act as physics labs with extreme conditions that cannot be replicated on Earth. A pulsar emits electromagnetic radiation along its magnetic axis. As the star rotates, we receive sequences of regular or discrete pulses when the brighter emission beam sweeps across the radio telescope. Most often, pulsars are found to possess stable rotation periods. Pulsar radio emissions typically exhibit three types of inherent single-pulse modulations: mode changing, nulling, and subpulse drifting. As for mode changing, it is known that a pulsar switches between two or more different stable emission states. Pulse nulling is an extreme phenomenon of mode changing, which is characterized by the absence of a single pulse. Nulling was first discovered by Backer (1970), and up to date, over 200 pulsars have been detected to exhibit pulse nulling (Sheikh & MacDonald 2021). The nulling fraction (NF) describes the proportion of time a pulsar behaves in a null state, with a likely minimum in the detected value of NF around 40%, which separates nulling pulsars into higher NF ones and lower NF ones (Konar & Deka 2019; Sheikh & MacDonald 2021). For most nulling pulsars, the NF is measured between 1% and 40%. However, there are extreme nulling pulsars, for example, PSR J1717−4054 possesses an NF of 95% (Wang et al. 2007). The duration of nulling follows an exponential distribution, suggesting a process with random Poisson points (Gajjar et al. 2017). Statistical analysis showed that NF is positively correlated with the pulsar period or characteristic age (Biggs 1992) and large NF is closely related to the spin period of the pulsar (Wang et al. 2020). PSR B0826−34 was the first pulsar to be detected with a weak emission pulse during the claimed null states (Esamdin et al. 2005; van Leeuwen & Timokhin 2012), and its weak mode intensity is only about 2% of that of the strong mode. Further investigation confirmed the existence of sporadic strong pulses during the weak state of the pulsar (Esamdin et al. 2012). Some pulsars exhibit periodic mode changes, such as PSR J1048−5832, which undergoes a periodic switch between strong and weak emission modes (Yan et al. 2020). Decades after the detection of pulse nulling, the physical mechanism of emission remains unclear. Several models have been proposed to try to explain the nulling phenomenon. They may originate from the change of

Table 1
Parameters of the Two Pulsars PSR J1611−0114 and PSR J1617+1123

Name	R.A.(J2000) (h:m:s)	Decl.(J2000) (d:m:s)	DM (pc cm^{-3})	P_0 (s)	Total Pulses
J1611−0114	16:11:55.0523	01:14:55.052	49.7	2.6	3617
J1617+1123	16:17:56.7295	11:23:23.8901	27.8	0.895	6937

distribution and continuous variation of current in the magnetosphere (Geppert et al. 2003). Such a phenomenon may also be caused by the cessation of radiation in the polar cap region (Ruderman & Sutherland 1975).

PSRs J1611−0114 and J1617+1123 were both discovered by the Commensal Radio Astronomy Five-hundred-meter Aperture Spherical radio Telescope (FAST) Survey. The 2.59 s pulsar J1611−0114 has a characteristic age of 10.1×10^6 yr, whereas J1617+1123 has a spin period of 0.895 s and a characteristic age of 47×10^6 yr. It was reported that J1611−0114 exhibits a pulse nulling phenomenon, and J1617+1123 shows obvious variation of emission (Wu et al. 2023), but detailed analyses are not presented. In this paper, we study the single-pulse properties and polarization characteristics of the two pulsars, PSRs J1611−0114 and J1617+1123, using FAST. Section 2 describes observations and data processing. Section 3 presents the data analysis results of these two pulsars, and Section 4 discusses and concludes the findings.

2. Observation and Data Processing

We conducted radio observations of PSRs J1611−0114 and J1617+1123 using FAST. The central beam of the 19-beam receiver was utilized with a frequency range of 1050–1450 MHz (Jiang et al. 2020). The data were recorded in search mode PSRFITS format with full polarizations, 1024 frequency channels, 8-bit digitization, and an interval of 49.152 μs. We observed J1611−0114 for 25 epochs. Among these, 7 observations lasted for 12 minutes and another 18 observations lasted for 4 minutes. For PSR J1617+1123, we also observed it for 25 sessions, each lasting 4 minutes. Their basic parameters are shown in Table 1.

In the offline analysis, we used DSPSR (Hotan et al. 2004) to extract single pulses with the ephemeris obtained by Wu et al. (2023). PAZ and PAZI tools in the PSRCHIVE software package were utilized to remove the radio frequency interference (RFI) from the data, where time-domain RFI was identified with the zero-dispersion measure (DM) matched filter, and frequency-domain RFI was recognized through the median smoothed difference algorithm and the mean offset rejection algorithm. A switched calibration signal with a period of 0.1006632960 s and a duration of 40 s was recorded prior to the pulsar observations. The rotation measure (RM) was determined using the RMFIT tool in the PSRCHIVE (Hotan et al. 2004), that is, the RM was obtained by fitting the variation trend of polarization angle across frequencies according to $\psi = \mathrm{RM}\lambda^2$, where λ is the radio wavelength corresponding to radio frequency ν. All the frequency channels and polarizations were scrunched to generate the total intensity with 512 phase bins per pulse period. Longitude-resolved fluctuation spectrum (LRFS) and two-dimensional fluctuation spectrum (2DFS) were calculated using the PSRSALSA package (Weltevrede 2016).

3. Results

3.1. Single-pulse Sequence and Energy Distribution

The single-pulse sequences from PSRs J1611−0114 and J1617+1123 are studied by analyzing and processing the obtained data. As shown in Figure 1, it displays the consecutive single-pulse stacks of the two pulsars in the main panel, the corresponding average pulse profiles in the upper panel and the corresponding relative energy variation in the right panel (PSR J1611−0114 on the left and PSR J1617+1123 on the right). The pulse sequence of J1611−0114 clearly shows the absence of emission between pulse numbers 36–44 and 60–65, which is known as the pulse nulling phenomenon. It suggests that J1611−0114 switches between a null state and a burst state. The integrated pulse profile depicted in the upper panel shows two components. The peak intensity of the first component is relatively weak, at about 75% of the peak intensity of the main pulse component. From the two-dimensional pulse stack of PSR J1617+1123, we can see that the pulse energy variation is more complicated, and its profile presents four emission components. The first and fourth components exhibit stronger emission intensity, with the peak intensity of the leading component being 60% of the trailing one. Meanwhile, the emission intensity of the central two components is slightly weaker, at ∼50% of the peak intensity.

We determine the phase range of the on-pulse region using the average pulse profile. The on-pulse region is defined as the range in which we detect significant pulsed emission over the whole longitude extent; that is, the emission intensity exceeds 3σ of the baseline. Then the phase-resolved intensities of the corresponding on-pulse window are summed to calculate the pulse energy of every single pulse. For the calculation of off-pulse energy, we choose the same window length as the pulse window length, select the stable baseline, and follow the

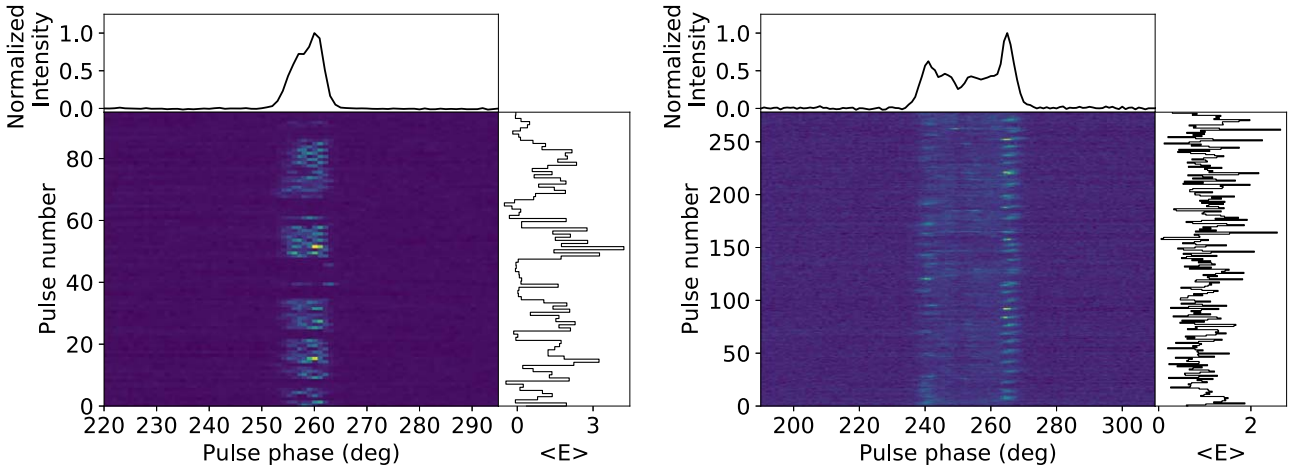

Figure 1. Two-dimensional single-pulse stack of pulsars J1611−0114 (left) and J1617+1123 (right) with corresponding average pulse profile in the upper panel and corresponding energy variation in the right panel. The observation dates were 2021 June 17 and 2021 July 21, respectively.

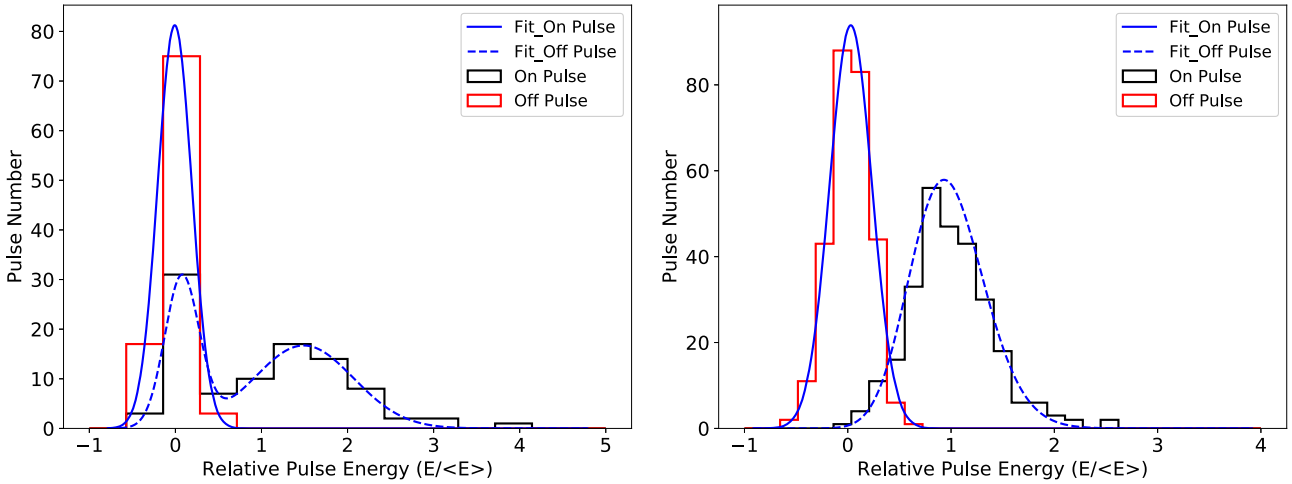

Figure 2. Energy distribution histograms for J1611−0114 (left) and J1617+1123 (right). The solid lines in red and black represent the off-pulse and on-pulse energy distributions respectively, while the dashed and solid lines in blue represent their corresponding fitting curves. Energy is normalized by average energy.

method described above to calculate the off-pulse energy of each single pulse. Figure 2 shows the energy distribution histograms of the two pulsars. The single-pulse energy for the on-pulse window after normalization by the mean pulse energy is indicated by the black histograms. From the left figure, it can be seen that the energy distribution of PSR J1611−0114 in the off-pulse region is obviously a Gaussian distribution, with the peak value at zero. The energy distribution in the on-pulse region shows a bimodal distribution, with peaks at 0.2 and 1.6, respectively, confirming the presence of pulse nulling for J1611−0114. We conduct a Kolmogorov–Smirnov (K-S) test on the double Gaussian distribution of on-pulse case and single Gaussian distribution of off-pulse case, obtaining their respective R_square values as 99.52% and 99.99%. The right panel shows the energy distributions of pulsar J1617+1123 in the on-pulse region and the off-pulse region. The energy distribution in the off-pulse region is a narrow Gaussian distribution with a peak value of 0. The energy distribution in the on-pulse region shows only a wide Gaussian distribution, with the peak deviating from zero. Therefore, there is no evidence of pulse nulling for J1617+1123.

3.2. Nulling Behavior

By utilizing the method introduced by Timokhin (2010), we distinguish the two states of null and burst by comparing the pulse energy with the threshold based on the system noise level. The uncertainty of the pulse energy is determined by $\sigma_{\rm ep} = \sqrt{n_{\rm on}}\sigma_{\rm off}$, where $n_{\rm on}$ represents the number of bins in the selected on-pulse window, and $\sigma_{\rm off}$ indicates the rms of the off-pulse region of a

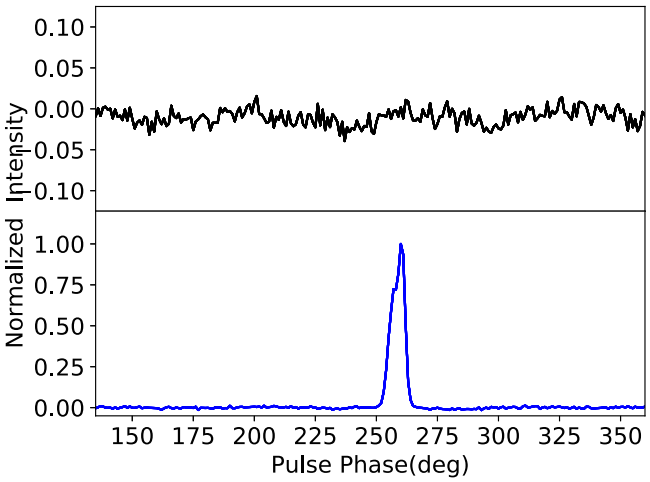

Figure 3. Average pulse profiles of J1611−0114 null (top panel) and burst (bottom panel) states.

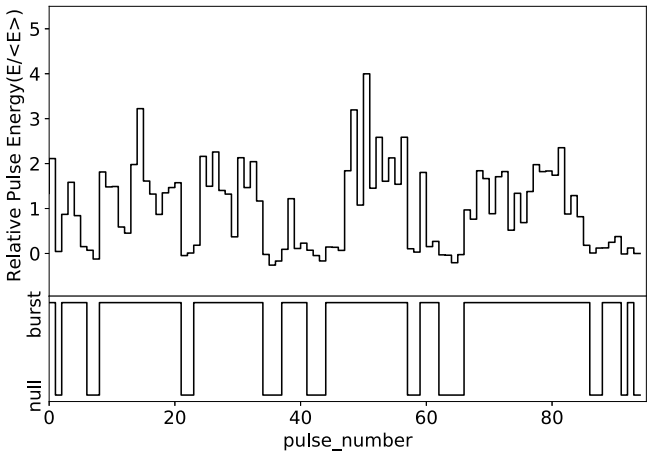

Figure 4. This diagram depicts the emission variation of J1611−0114. The upper panel shows the pulse energy, and the lower panel shows the corresponding null and burst states.

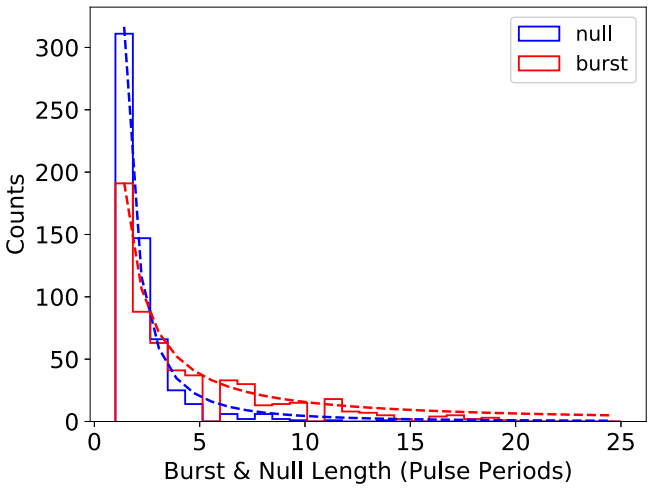

Figure 5. Histograms of the duration distributions of null and burst states of J1611−0114. The dashed blue line in the figure represents the power-law fitting to null duration. The dashed red line in the figure represents the power-law fitting to burst duration.

single pulse. Due to the high sensitivity of FAST, we chose $3\sigma_{\rm ep}$ as the threshold. Pulses with energies lower than this threshold are classified as nulling pulses, while those above are classified as burst pulses. In order to more accurately identify the null and burst states, we perform a manual intervention. If there is a burst pulse within the continuous nulling pulse, we classify burst pulse as a nulling pulse.

The NF is a fundamental parameter used to describe the nulling phenomenon. The method proposed by Ritchings (1976) is employed to estimate the NF of pulsar J1611−0114. The error of NF is usually calculated as $\sqrt{n_p}/n$, where n_p is the number of nulling pulses and n is the total number of observed pulses (Wang et al. 2007). The NF values of 25 observations were determined using the method described above, with distribution between 30% and 50% and an average NF value of $40.1\% \pm 5.4\%$. The NF values obtained from observations are mainly distributed between 30% and 50%, with slight variations. These slight variations of NF values may be caused by the shorter duration of observations on PSR J1611−0114 and the fluctuating amount of nulling pulses observed each epoch. By combining the data from all sessions, the NF value for all observations is calculated to be $39.8\% \pm 2.7\%$, which indicates a better evaluation of the nulling behavior.

In order to investigate whether the observed null pulse is a weak emission pulse or not, we folded the pulses of the null state and the burst state to obtain the average pulse profiles, respectively, as shown in Figure 3 in the upper and lower panels. The upper panel displays the average pulse profile of the null state, while the lower panel shows the average pulse profile of the burst state. We find that there is no significant radiation component greater than $3\sigma_{\rm ep}$ in the upper panel. Therefore we believe that the null pulse identified by $3\sigma_{\rm ep}$ as the threshold is not indicative of weak radiation.

As depicted in Figure 4, the observed pulse energy of J1611−0114 and its corresponding null state or burst state are plotted. The horizontal coordinate represents the number of pulses. We utilized the method described by Gajjar et al. (2017) to investigate the periodicity of the nulling phenomenon of PSR J1611−0114. Specifically, we conducted a Fourier transform on the identified null pulse and burst pulse, assigning a value of 1 to the burst pulse and 0 to the nulling pulse. However, our analysis did not reveal any periodicity in the pulsar, indicating that the nulling phenomenon does not occur periodically in our data set. Figure 5 illustrates the histogram of the duration distribution of all observed data corresponding to

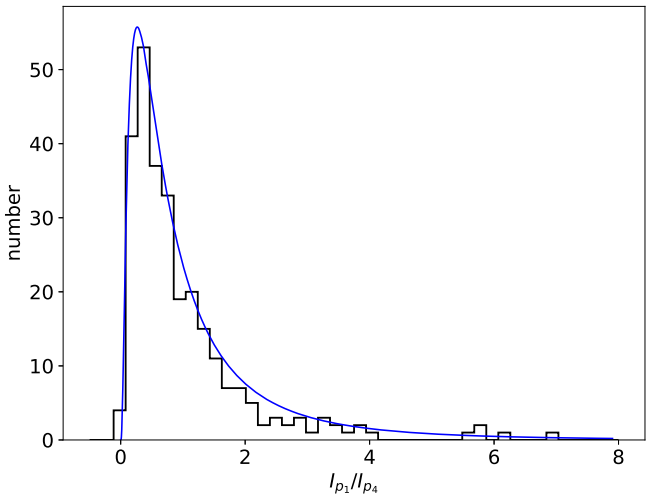

Figure 6. Histograms of the first and fourth component peak-to-maximum ratios for J1617+1123.

both the null and burst states of PSR J1611−0114. It is evident from the figure that the durations for null and burst states span 1–9 pulse cycles and 1–22 pulse cycles, respectively. The duration distributions for null and burst states in the figure exhibit approximately power-law behavior, with power indices of around 2.2 ± 0.1 and 1.28 ± 0.05, respectively.

The single pulse sequence diagram and energy distribution histogram of J1617+1123 show that there is no nulling phenomenon. In Figure 1, it can be seen from the single pulse sequence diagram of J1617+1123 that the pulse intensity of the fourth component is noticeably stronger than that of the first component. However, there are also instances where the pulse intensity of the first component exceeds that of the fourth component. In order to determine whether J1617+1123 has two different modes, we divide the pulses into four components. We search for the peak values of the first and fourth components for each pulse, and calculate the ratio of the two peak values. As shown in Figure 6, the histogram of the ratios is plotted. It can be seen from the graph that the distribution of the peak value ratios follows a log-normal distribution. It implies that there are no two states, indicating that J1617+1123 does not exhibit mode changes in short-term scale observations.

3.3. Single-pulse Modulation

As shown in Figure 7, to investigate the behavior of pulse modulation, we have plotted the LRFS (Backer 1970), 2DFS (Edwards & Stappers 2002) and the modulation index distribution. LRFS is used to determine whether the pulse intensity changes periodically over time. It is calculated by dividing the pulse stack into pulse blocks of the same size and performing a Fast Fourier Transform on these blocks (Serylak et al. 2009). Then, the fluctuating power spectrum of different blocks is averaged to obtain the final fluctuation spectrum. 2DFS is used to analyze whether a single pulse sequence exhibits subpulse drift in the longitude direction (Edwards & Stappers 2003). Similar to the calculation method of LRFS, the two-dimensional discrete Fourier transform can be applied to longitude-time data. In this case, the result of the computation along columns is known as the LRFS, and the spectrum of rows represents the drift period of the subpulse in the longitude direction. Both the LRFS and 2DFS are horizontally integrated, producing the side-panels of the spectra, which correspond to P_0/P_3 in the case of drifting subpulses. The power in the 2DFS is vertically integrated, producing the bottom plots, which correspond to P_0/P_2 in the case of drifting. In this context, P_0 signifies the spin period, P_2 denotes the horizontal distance between subpulse drift bands on the pulse longitude and P_3 indicates the periodicity of pulse intensity modulation.

In Figure 7, the plots of LRFS for the two pulsars are presented in the middle panels, the 2DFS plots are shown in the bottom panels, and the top panels display the modulation index distribution. It can be seen from the LRFS diagram that J1611−0114 exhibits modulation characteristics, with modulation period of 2.01 ± 0.01 $P_0 (P_3 \approx 2P_0)$. The values of P_3 are consistent in each observation. In the 2DFS diagram, it is evident that there is no indication of subpulse drifting. We detect the pulse even–odd modulation feature (Wang et al. 2023). As shown in the pulsar's single pulse sequences (Figure 1), the subpulses appear at the same pulse longitude every other rotation cycle. For PSR J1617+1123, the presence of the modulation period is clearly visible in the LRFS plot. By measuring the modulation period (P_3) value of each observation, it is found that the value of P_3 obtained from each observation is slightly different. Figure 8 shows P_3 at different epochs in the left figure, and the statistics of P_2 and P_3 in the right figure. It can be seen from the left figure that the value of P_3 ranges from 6.29 ± 0.24 P_0 to $10.39 \pm 0.33 P_0$, with an average value of $8.01 \pm 0.24 P_0$. The primary panel on the right depicts the scatter plots observed for P_3 and P_2. The upper panel and the side panel display the statistical histograms (probability density function, PDF) for P_3 and P_2, correspondingly, with their respective fitted Gaussian distributions depicted with solid blue lines. For PSR J1617+1123, it is clear from the figure that the modulation period exists.

It is evident from Figure 7 that the peak of P_0/P_2 is at 12, indicating that subpulse drifting has been detected in this pulsar. We analyzed the 2DFS plots of the two components with higher intensity, as shown in Figure 9. The panel on the left features the 2DFS diagram of the first component. It can be seen that its modulation period is relatively scattered, with the peak value of P_3 at 12.67 ± 0.35 P_0. There is no indication of drifting for the first component. The panel on the right displays the 2DFS diagram of the fourth component, with a modulation period of 8.04 ± 0.39 P_0. In the 2DFS diagram, it can be clearly seen that the peak value of P_2/P_0 for the fourth component is at

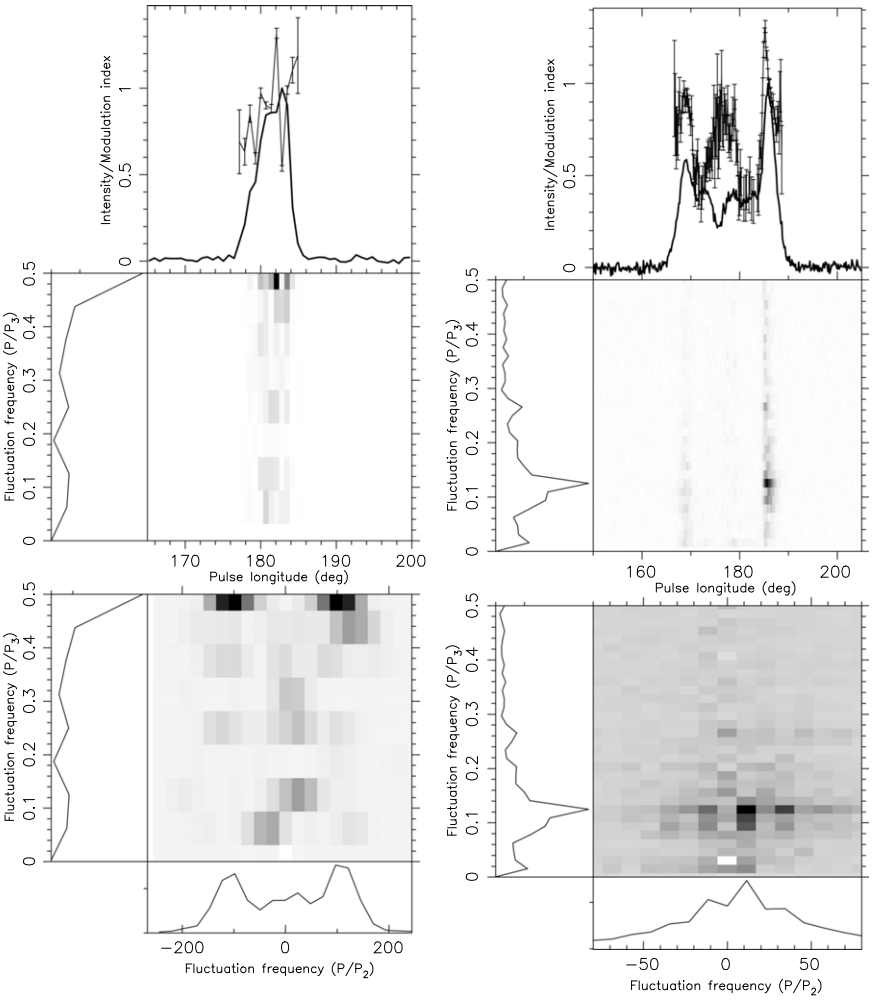

Figure 7. LRFS and 2DFS of J1611−0114 and J1617+1123.

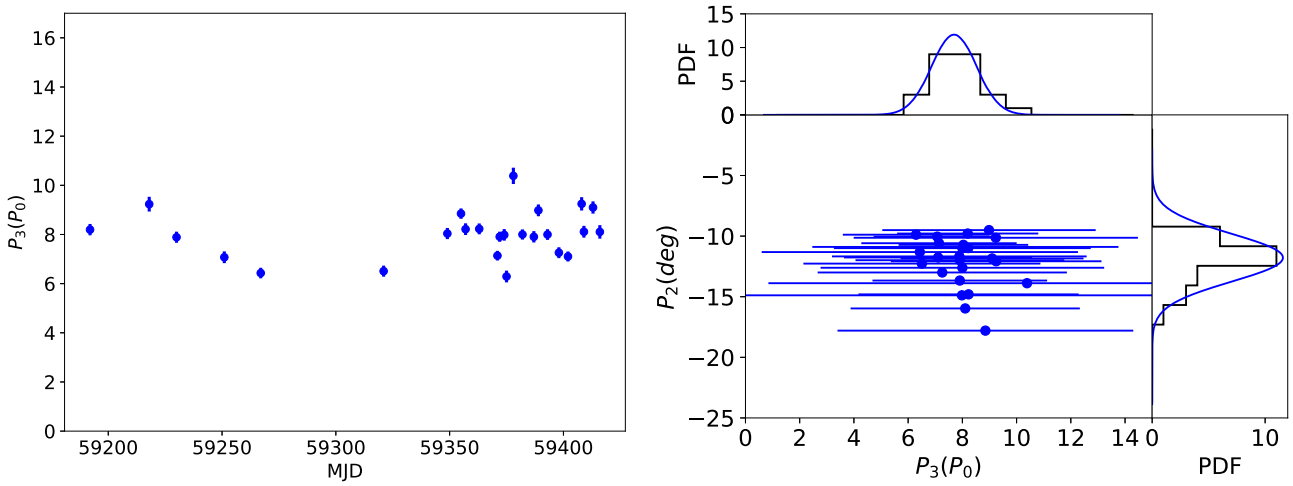

Figure 8. The relationship between P_3 and epoch in J1617+1123, and the statistics of P_2 and P_3. The main panel on the right is a scatter plot of the P_2 and P_3 values determined in our observations. The PDFs for P_3 and P_2 are displayed in the top panel and the right panel, respectively.

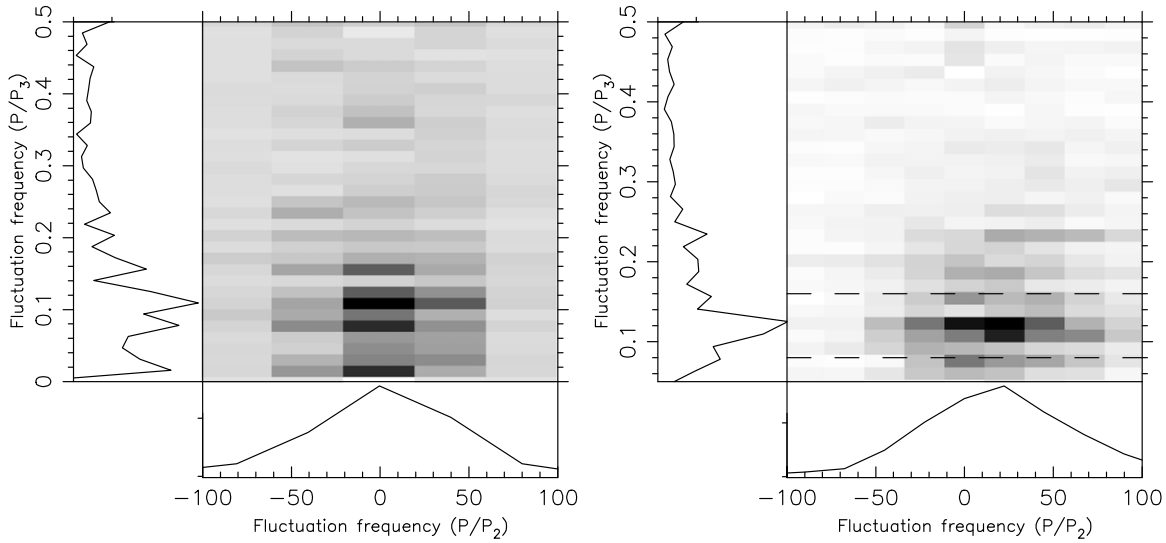

Figure 9. 2DFS plot of the first and last components for J1617+1123. The left panel shows the 2DFS plot for the first component and the right panel shows the 2DFS plot for the fourth component. The observation date was 2021 July 21.

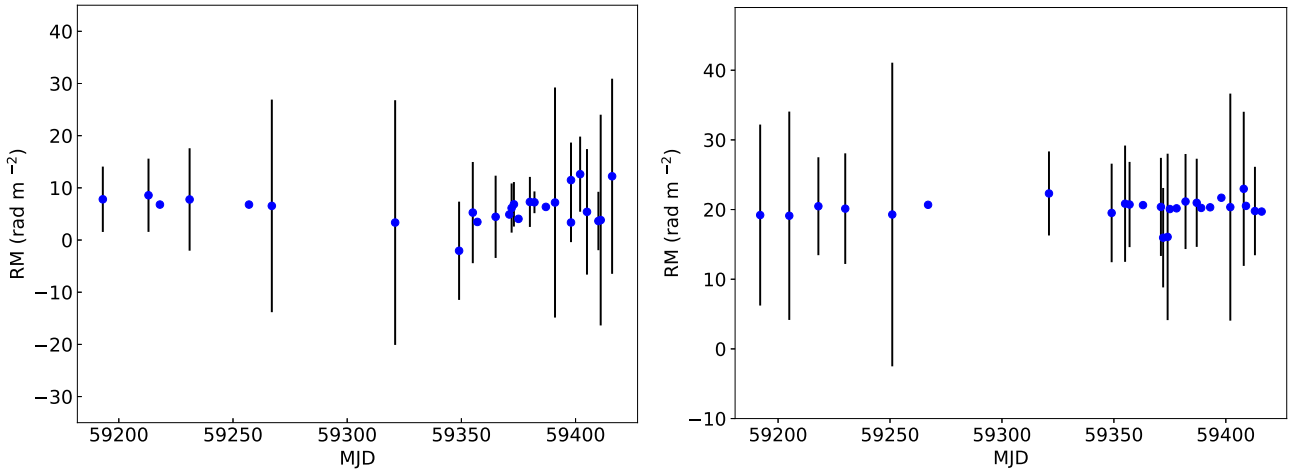

Figure 10. RM at various epochs for J1611−0114 (left) and J1617+1123 (right). The blue dots with black error bars stand for RM.

about 24 pulses, which suggests that there is a phenomenon of subpulse drifting.

The longitude-resolved modulation index (LRMI) reflects the intensity change of the pulse at a given pulse phase position, defined as $m = \frac{\sqrt{\sigma_{\rm on}^2 - \sigma_{\rm off}^2}}{\langle I \rangle}$ where $\sigma_{\rm on}$ and $\sigma_{\rm off}$ are the rms of on-pulse intensity and off-pulse intensity respectively, and I is the on-pulse intensity. We present the LRMI in the top panels of Figure 7. The LRMI values for PSR J1611−0114 range from 0.5 to 1.3. It is clear that the LRMI shows a significant drop at the peak of the right component. While toward its trailing edge, the LRMI values increase. For J1617+1123, the LRMI exhibits a "W" shape across the pulse phase, with LRMI values ranging between 0.5 and 1.0. This indicates a relatively high variability in the intensity of the outer components.

3.4. Polarization Characteristics

With the aim of characterizing the polarization of pulsars, we utilize PSRCHIVE to perform polarimetric calibration on the observed data. The optimal RM values are obtained from the RMFIT routine in the PSRCHIVE software package. Figure 10 shows the temporal evolution of RM. The observed RM of J1611−0114 ranges from −3.0 to 15.0 rad m^{-2}, with an average value of 6.2 ± 7.9 rad m^{-2}. For J1617+1123, the RM ranges from 15.0 to 25.0 rad m^{-2}, with an average value of 20.1 ± 6.3 rad m^{-2}. RM of the Earth's ionosphere is not included. The four Stokes

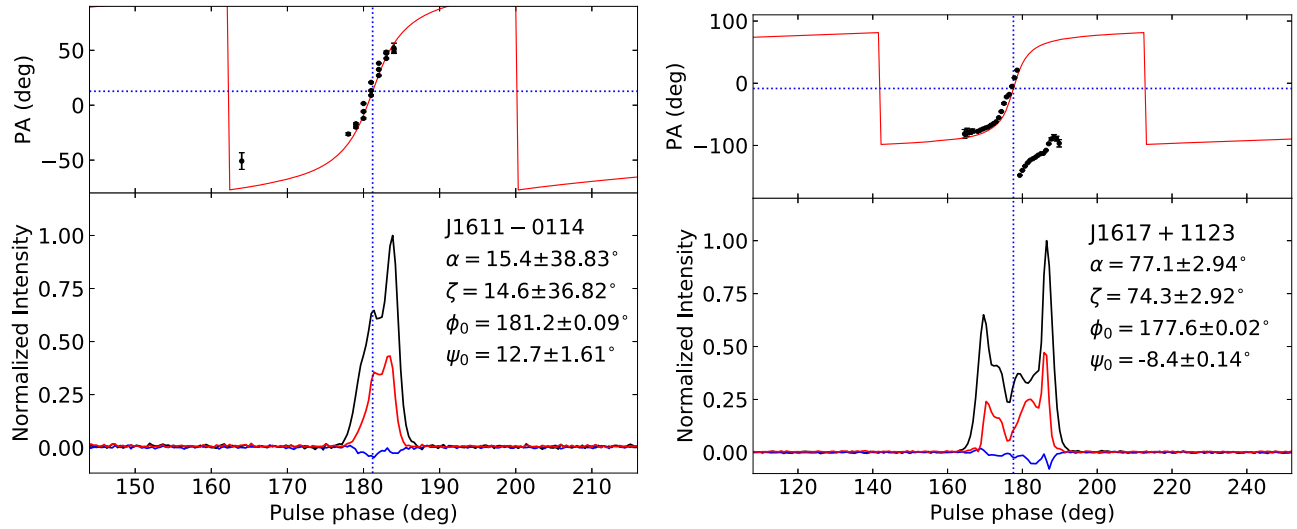

Figure 11. The polarization profile of J1611−0114 (left) and J1617+1123 (right). In the bottom panels, the solid lines in black, red, and blue indicate the total, linear, and circular polarization intensities, respectively. The black dots with error bars on the left upper panel are the polarization PA.

parameters, I (total intensity), Q, U, and V (circular polarization), can be obtained directly from radio observations of pulsars through polarization calibration. The polarized average pulse profiles are obtained by integrating over time and frequency domains, where the linear polarization intensity is $L = (Q^2 + U^2)^{\frac{1}{2}}$. Figure 11 displays the polarization profiles of PSRs J1611−0114 and J1617+1123. The panel on the left is obtained by averaging all the observed polarization results. PSRs J1611−0114 and J1617+1123 have linear polarization fractions of $40.56\% \pm 1.11\%$ and $38.89\% \pm 2.80\%$, and circular polarization rates of $-3.61\% \pm 0.48\%$ and $-4.31\% \pm 0.87\%$, respectively. The panel at the top of Figure 11 corresponds to the linear polarization position angle (PA) curve, which exhibits a distinct "S" shape. For PSR J1611−0114, its profile has two components, with the first component being not obvious, and the linear polarization curve is similar to the pulse curve. To constrain geometric parameters, a grid search is performed in magnetic inclination angle (α) and impact angle (β). Then the minimum χ^2 fit between the rotating vector model (RVM) curve and the data is determined by optimizing the remaining free parameters ϕ_0 and ψ_0, where PA (ψ_0) as a function of the pulsar's longitude is $\tan(\psi - \psi_0) = \frac{\sin(\phi - \phi_0)\sin\alpha}{\sin\zeta\cos\alpha - \sin\alpha\cos\zeta\cos(\phi - \phi_0)}$, where $\zeta = \alpha + \beta$ is the angle between the axis of rotation and the line of sight (Wang et al. 2023). Each rotation period of PSRs J1611−0114 and J1617+1123 utilizes 1024 and 512 bins, respectively, for the calculation of χ^2. The resulting values correspond to surfaces in the (α, β) space, as depicted in Figure 12. Three contours representing the 1σ, 2σ, and 3σ uncertainties in α and β are provided.

We align all the average profiles observed at each epoch and sum them to obtain the standard profile. Then we compare the standard profile with the average profiles by calculating the residuals. By examining the residual plots, we find that the pulse of the observed pulsars is unstable. We divided all observation data into two sub-bands with center frequencies of 1150 MHz and 1350 MHz respectively. The pulse profiles of these two sub-bands are shown in Figure 13. It can be seen that the pulse profile shapes of PSRs J1611−0114 and J1617+1123 at 1150 and 1350 MHz are slightly different. For J1611−0114 in Figure 13 on the left, the leading component at 1150 MHz is wider than that at 1350 MHz, and the peak value of the first component at 1150 MHz is lower than that at 1350 MHz. For J1617+1123 in Figure 13 on the right, it can be seen that the intensities of the first component and the middle two components change significantly, with higher intensities at 1250 MHz than at 1150 and 1350 MHz. However, the pulse width remains unchanged.

4. Discussion and Conclusions

This paper describes the single pulse studies of two pulsars, J1611−0114 and J1617+1123, using FAST at the central frequency of 1250 MHz. PSR J1611−0114 shows evidence of the pulse nulling phenomenon from the bimodal distribution of pulse energy. The nulling duration approximately presents a power-law distribution, which is suggested to be related to the randomness in the radiation process and the changes of pulsar magnetosphere (Cordes & Shannon 2008). The NF has been regarded as an important parameter for characterizing the pulse nulling phenomenon in pulsars, and was found to be correlated with the pulsar age or rotational period (Ritchings 1976; Biggs 1992; Wang et al. 2007). PSR J1611−0114 has a long period of 2.6 s, and the average NF of PSR J1611−0114 is estimated to be around 40.1%. No emission in the average

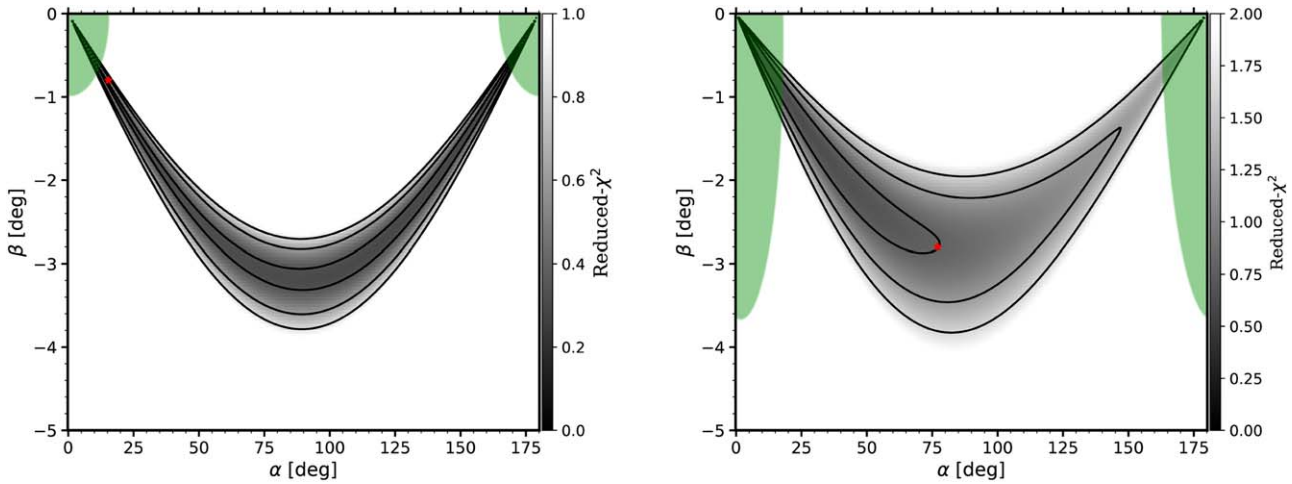

Figure 12. The surfaces of magnetic inclination angle (α) and impact angle (β) for J1611−0114 (left) and J1617+1123 (right). The figure shows the reduced chi-square (χ^2) surface as gray scale, with black contours corresponding to 1σ, 2σ and 3σ significance levels. The red dots are the most probable fitting values for the α and β. The green areas show the viewing geometries constrained by the observed pulse width.

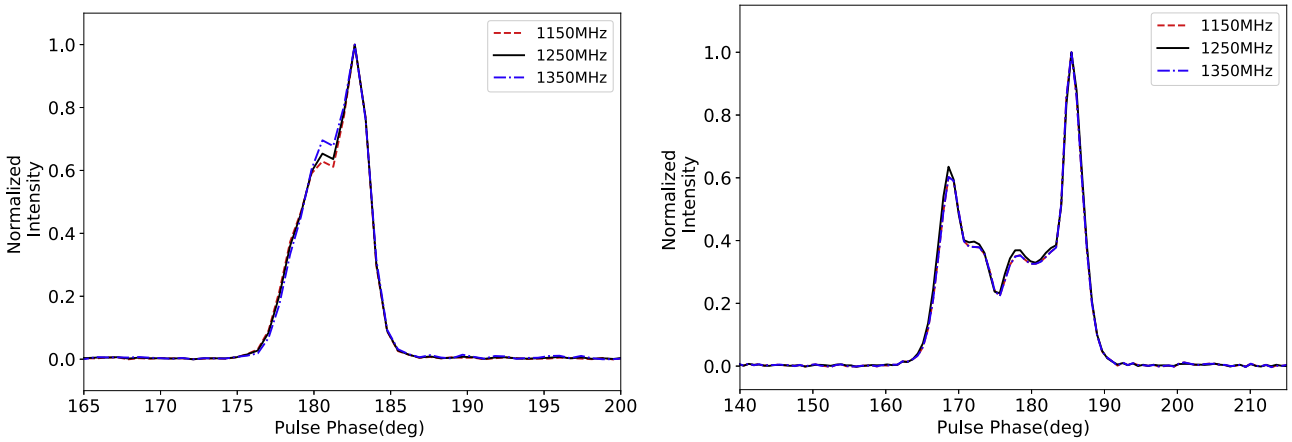

Figure 13. Pulse profiles of J1611−0114 (left) and J1617+1123 (right) in the 1150 and 1350 MHz sub-bands.

pulse profile integrated over all null pulses is detected with significance above 3σ. Han & Yuen (2022) reported that nulling pulsars typically exhibit a duty cycle of 0.1 or lower and are likely to have small obliquity angles. For PSR J1611−0114, the duty cycle and magnetic inclination angle are calculated to be 0.018 and 37°.6, respectively. Currently, the physical origins of pulse nulling remain a mystery. Explanations include the absence of line of sight (Herfindal & Rankin 2007) and changes in radiation mechanisms (Zhang & Cheng 1997). Changes in the magnetospheric state, such as alterations in magnetospheric geometry or current, may shift the line-of-sight direction corresponding to the pulsar's radiation beam (Timokhin 2010). Pulse nulling may also occur when radiation from the polar cap is obstructed (Ruderman & Sutherland 1975), or when an orbiting companion blocks the line of sight (Cordes & Shannon 2008).

Through the analysis of fluctuation spectra, PSR J1611−0114 shows the presence of a modulation feature with a periodicity of 2.23 ± 0.02 s, which is raised from the periodic amplitude modulation. The trailing component of PSR J1617+1123 exhibits significant subpulse drifting with estimated periodicity of 10 rotational periods. Subpulse drifting is considered to be prevalent, with estimations suggesting that over half of the entire pulsar population displays this phenomenon (Weltevrede et al. 2007). Basu et al. (2020) have reported an association between subpulse drifting and spin-down luminosity ($\dot{E}$). Drifting is exclusively detected in pulsars with $\dot{E} < 2 \times 10^{32}$ erg s^{-1}. In the case of J1617+1123, its $\dot{E}$ is

measured to be 1.7×10^{31} erg s^{-1}, aligning with the statistics provided by Basu et al. (2020). It has been found that the least energetic pulsars tend to exhibit larger values of drifting periodicity (P_3), with a weak anti-correlation between drifting periodicity (P_3) and $\dot{E}$ (Basu et al. 2020). Song et al. (2023) reported that larger P_3 values are associated with older pulsars with lower spin-down power, as well as more energetic young pulsars, while the lowest P_3 values are predominant at approximately $\tau_c \approx 3.2 \times 10^7$ yr (or $\dot{E} \approx 3.2 \times 10^{31}$ erg s^{-1}). Regarding J1617+1123, it possesses a characteristic age of 4.7×10^7 yr and $\dot{E}$ of 1.7×10^{31} erg s^{-1}, which is approximately consistent with the prediction. Furthermore, the detection of subpulse drifting in PSR J1617+1123 is consistent with the previous conclusion that the subpulse drifting is only confined to the pulse profile's cone component, and the core component never displays such modulation (Basu et al. 2020). Some pulsars show a strong correlation between pulse nulling and mode changes. For instance, PSR B0826–34 exhibits different modes with varying pulse profiles during nulling phenomena (Esamdin et al. 2005). It is noted that pulsar J1611−0114 may undergo a significant mode change in its average pulse profile. The mode change may be accompanied by changes in the timing behaviors of the pulsar over long timescales. The long-term emission-rotation correlation seen in some pulsars suggests that the changing currents of charged particles in the pulsar magnetosphere are responsible for both emission changes and variations in braking torque (Lyne et al. 2010). It is suggested that the patterns arise through beats between the magnetospheric drift and interaction of widely separated regions of the magnetosphere (Wright 2022). Further studies of emission properties of more pulsars are helpful to comprehend the origin of the various patterns.

Acknowledgments

This work is supported by National Key Research and Development Program of China (2022YFC2205203), the Major Science and Technology Program of Xinjiang Uygur Autonomous Region (No. 2022A03013-1), and the National Natural Science Foundation of China (NSFC, grant Nos. U1838109 and 12041304). Z.G.W. is supported by the Major Science and Technology Program of Xinjiang Uygur Autonomous Region (No. 2022A03013-1), the National Natural Science Foundation of China (NSFC, Grant No. 12303053), the 2021 project Xinjiang Uygur autonomous region of China for Tianshan elites, the Youth Innovation Promotion Association of CAS under No. 2023069, and the Tianshan Talent Training Program (No. 2023TSYCCX0100). W.M.Y. is supported by the National SKA Program of China (grant No. 2020SKA0120200), the National Natural Science Foundation of China (NSFC, grant Nos. 12041303, 12273100 and 12288102), the National Key R&D Program of China (grant No. 2022YFC2205201), the West Light Foundation of the Chinese Academy of Sciences (grant No. WLFC 2021-XBQNXZ-027), and the Major Science and Technology Program of Xinjiang Uygur Autonomous Region (grant No. 2022A03013-4).

References

Backer, D. C. 1970, Natur, 228, 42
Basu, R., Mitra, D., & Melikidze, G. I. 2020, ApJ, 889, 133
Biggs, J. D. 1992, ApJ, 394, 574
Cordes, J. M., & Shannon, R. M. 2008, ApJ, 682, 1152
Edwards, R. T., & Stappers, B. W. 2002, A&A, 393, 733
Edwards, R. T., & Stappers, B. W. 2003, A&A, 407, 273
Esamdin, A., Abdurixit, D., Manchester, R. N., & Niu, H. B. 2012, ApJL, 759, L3
Esamdin, A., Lyne, A. G., Graham-Smith, F., et al. 2005, MNRAS, 356, 59
Gajjar, V., Yuan, J. P., Yuen, R., et al. 2017, ApJ, 850, 173
Geppert, U., Rheinhardt, M., & Gil, J. 2003, A&A, 412, L33
Han, X. H., & Yuen, R. 2022, ApJ, 940, 110
Herfindal, J. L., & Rankin, J. M. 2007, MNRAS, 380, 430
Hotan, A. W., van Straten, W., & Manchester, R. N. 2004, PASA, 21, 302
Jiang, P., Tang, N.-Y., Hou, L.-G., et al. 2020, RAA, 20, 064
Konar, S., & Deka, U. 2019, JApA, 40, 42
Lyne, A., Hobbs, G., Kramer, M., Stairs, I., & Stappers, B. 2010, Sci, 329, 408
Ritchings, R. T. 1976, MNRAS, 176, 249
Ruderman, M. A., & Sutherland, P. G. 1975, ApJ, 196, 51
Serylak, M., Stappers, B. W., & Weltevrede, P. 2009, A&A, 506, 865
Sheikh, S. Z., & MacDonald, M. G. 2021, MNRAS, 502, 4669
Song, X., Weltevrede, P., Szary, A., et al. 2023, MNRAS, 520, 4562
Timokhin, A. N. 2010, MNRAS, 408, L41
van Leeuwen, J., & Timokhin, A. N. 2012, ApJ, 752, 155
Wang, H., Wen, Z. G., Duan, X. F., et al. 2023, ApJ, 950, 166
Wang, N., Manchester, R. N., & Johnston, S. 2007, MNRAS, 377, 1383
Wang, P. F., Han, J. L., Han, L., et al. 2020, A&A, 644, A73
Weltevrede, P. 2016, yCat, J/A+A/590/A109
Weltevrede, P., Stappers, B. W., & Edwards, R. T. 2007, A&A, 469, 607
Wright, G. 2022, MNRAS, 514, 4046
Wu, Q. D., Yuan, J. P., Wang, N., et al. 2023, MNRAS, 522, 5152
Yan, W. M., Manchester, R. N., Wang, N., et al. 2020, MNRAS, 491, 4634
Zhang, L., & Cheng, K. S. 1997, ApJ, 487, 370